

Target effects in negative-continuum assisted dielectronic recombination

V. A. Yerokhin,^{1,2} A. N. Artemyev,³ V. M. Shabaev,⁴ Th. Stöhlker,^{2,5} A. Surzhykov,² and S. Fritzsche^{2,6}

¹Center for Advanced Studies, Peter the Great St. Petersburg Polytechnic University, Polytekhnicheskaya 29, 195251 St. Petersburg, Russia

²Helmholtz-Institut Jena, Fröbelstieg 3, D-07743 Jena, Germany

³Institut für Physik, Universität Kassel, Heinrich-Plett-Str. 40, 34132, Kassel, Germany

⁴Department of Physics, St. Petersburg State University, Ulianovskaya 1, Petrodvorets, St. Petersburg 198504, Russia

⁵Institut für Optik und Quantenelektronik, Friedrich-Schiller-Universität Jena, 07743 Jena, Germany

⁶Theoretisch-Physikalisches Institut, Friedrich-Schiller-Universität Jena, Fürstengraben 1, 07743 Jena, Germany

The process of recombination of a quasi-free electron into a bound state of an initially bare nucleus with the simultaneous creation of a bound-electron-free-positron pair is investigated. This process is called the negative-continuum assisted dielectronic recombination (NCDR). In a typical experimental setup, the initial electron is not free but bound in a light atomic target. In the present work, we study the effects of the atomic target on the single and double-differential cross sections of the positron production in the NCDR process. The calculations are performed within the relativistic framework based on QED theory, with accounting for the electron-electron interaction to first order in perturbation theory. We demonstrate how the momentum distribution of the target electrons removes the non-physical singularity of the differential cross section which occurs for the initially free and monochromatic electrons.

PACS numbers: 34.10.+x, 34.50.Fa

I. INTRODUCTION

One of the main processes that occurs in the collision of an electron with a bare nucleus is the radiative recombination of the electron into a bound state under the simultaneous emission of a photon [1, 2]. If the energy of the initial electron is high enough, new recombination channels become energetically possible. In the present work we are interested in one of these channels in which the recombination of the initial electron leads to the creation of an electron-positron pair. The electron from this pair is captured into a bound state of the ion, whereas the positron is emitted into the continuum. Such process is called the *negative-continuum assisted dielectronic recombination* (NCDR) [3, 4],

$$X^{Z+} + e^- \rightarrow X^{(Z-2)+} + e^+. \quad (1)$$

We refer here to the analogy between NCDR and the well-known dielectronic recombination (DR) [5–9]. The difference between the two processes is that in DR the second electron is excited from an initially bound state, whereas in NCDR it is “excited” from the negative continuum.

In contrast to the dielectronic recombination, NCDR is a nonresonant process, with the energy threshold condition

$$T_i \geq 2mc^2 - E_{\text{io}}(a) - E_{\text{io}}(b), \quad (2)$$

where T_i is the kinetic energy of the initial-state electron in the nucleus rest frame, m is the electron mass, and $E_{\text{io}}(a)$ and $E_{\text{io}}(b)$ are the ionization energies of the first and second electron in the final state, respectively. For the bare uranium nucleus, the threshold energy is $T_i \approx 760$ keV.

The NCDR process has a distinct signature that facilitates its experimental identification, namely, the coincidence of the emitted positron with the doubly charge-exchanged ion. Other possible (two-step) processes that result in the same final state of the ion and positron were shown [11] to yield much smaller

contributions, well below of what can be resolved under the present and near-future experimental conditions. The NCDR has not been observed until now but should become accessible at the High-Energy Storage Ring (HESR) facility at the future FAIR acceleration complex. Indeed, such experiments are planned [17]; a first feasibility study has been presented in Ref. [10].

Theoretical investigations of the NCDR process have been carried out in Refs. [3, 4] under the assumption that the initial-state nucleus X^{Z+} is colliding with the monochromatic electron beam. The presently prepared experiments, however, are going to use a somewhat different scenario [10]. In it, a heavy energetic bare nucleus will collide with a light atomic target A (which is at rest in the laboratory frame). For appropriate collision energies, the nucleus can capture one electron from the target, while another electron is excited from the negative continuum, producing a positron in continuum,

$$X^{Z+} + A \rightarrow X^{(Z-2)+} + A^+ + e^+. \quad (3)$$

Here we aim to analyze the NCDR process within this scenario that may be realized in a future experimental setup at the HESR.

In practice, the atomic target affects the NCDR process in a two-fold manner. Firstly, it determines the shape of the energy spectra of the emitted positron; secondly, it removes the nonphysical singularity of the angle-differential NCDR cross section in the laboratory frame as reported in Refs. [3, 4]. In the present work we shall consider both these effects in detail.

The paper is organized as follows. Section II describes the theory of the NCDR process within the relativistic framework. Numerical details are discussed in Sec. III. Sec. IV presents the results and discussion. Finally, a short summary is given in Sec. V. Relativistic units $\hbar = c = 1$ are used throughout the paper.

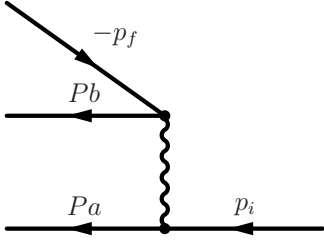


FIG. 1: Schematic representation of the negative-continuum assisted dielectronic recombination. p_i denotes the incoming quasi-free electron, $-p_f$ represents the outgoing positron, a and b are bound one-electron states, and P is the permutation operator, $PaPb = ab$ or ba .

II. THEORY

A. Monochromatic initial-state electrons

We start from the same scenario of monochromatic initial-state electrons as was considered previously in Refs. [3, 4]. In the rest frame of the nucleus, the incoming electron possesses the asymptotic momentum \mathbf{p}_i , the energy $\varepsilon_i = (\mathbf{p}_i^2 + m^2)^{1/2}$, and the helicity $m_i = \pm 1/2$. In the final state we have a continuum positron with the asymptotic momentum \mathbf{p}_f , energy $\varepsilon_f = (\mathbf{p}_f^2 + m^2)^{1/2}$, and the momentum projection m_f as well as the two-electron bound state $|n_a \kappa_a, n_b \kappa_b; JM\rangle$ with the total angular momentum J and projection M . Here, n_a , κ_a and n_b , κ_b denote the principal quantum number and the relativistic angular quantum number of the electrons states a and b , respectively.

Following the general QED theory [14] (see also Refs. [3, 4]), the angle-differential cross section of the NCDR process in the nucleus-rest frame is given by

$$\frac{d\sigma}{d\Omega_f} = \frac{16\pi^4 N^2}{v_i} \varepsilon_f |\mathbf{p}_f| \sum_{m_i m_f M} \left| \sum_{m_a m_b} C_{j_a m_a, j_b m_b}^{JM} \right|^2 \times \sum_P (-1)^P \langle PaPb | I(\varepsilon_i - \varepsilon_{Pa}) | p_i m_i, -p_f m_f \rangle \quad (4)$$

where v_i is the speed of the incoming electron, P is the permutation operator, $PaPb = (ab)$ or (ba) , $(-1)^P$ is the sign of the permutation, $|ab\rangle \equiv |n_a \kappa_a m_a, n_b \kappa_b m_b\rangle$; $N = 1/2$ when $n_a = n_b$ and $\kappa_a = \kappa_b$ and $N = 1/\sqrt{2}$ otherwise; ε_a and ε_b are the one-electron energies of the electron states a and b , respectively; $|pm\rangle$ denotes the electron continuum Dirac state with a definite asymptotic 4-momentum $p \equiv (\varepsilon, \mathbf{p})$ and a momentum projection m , and $I(\omega)$ is the relativistic operator of the electron-electron interaction. In the Feynman gauge, $I(\omega)$ reads

$$I(\omega) = \alpha (1 - \boldsymbol{\alpha}_1 \cdot \boldsymbol{\alpha}_2) \frac{\exp(i|\omega|r_{12})}{r_{12}}, \quad (5)$$

where α denotes the fine-structure constant, $r_{12} = |\mathbf{r}_1 - \mathbf{r}_2|$ is the distance between the electrons, and $\boldsymbol{\alpha}_k$ denotes the vector of Dirac matrices acting on the k th electron.

In Eq. (4) we have assumed that the incident electron is unpolarized and that the spin states of the emitted positron as well as the momentum projections of the residual ion remain unobserved. Following the standard procedure [12, 13], we have replaced the positron with four-momentum p_f and momentum projection m_f by an electron with four-momentum $-p_f$ and momentum projection $-m_f$. Fig. 1 displays this process schematically in terms of its Feynman diagram.

Eq. (4) is exact in leading order of QED perturbation theory with regard to the electron-electron interaction. Higher-order electron-electron interaction effects are suppressed typically by a parameter of $1/Z$, where Z is the nuclear charge of the projectile. For heavy projectiles, as those considered in the present work, these effects are small and negligible.

The energy of the emitted positron in Eq. (4) is fixed by the energy conservation condition (in the rest frame of the nucleus),

$$\varepsilon_f = \varepsilon_i - \varepsilon_a - \varepsilon_b, \quad (6)$$

or

$$T_f = T_i - 2m + E_{\text{io}}(a) + E_{\text{io}}(b), \quad (7)$$

where $E_{\text{io}}(a)$ and $E_{\text{io}}(b)$ are the ionization energies of the electrons a and b , respectively. Within the approximation of Eq. (4), the final-state electrons a and b are considered within the independent particle model, so the energy of the final bound state of the helium-like ion is given by the sum of the Dirac energies of the electrons a and b .

It should be noted that Eq. (4) differs from the analogue formulas in Refs. [3, 4] by the prefactor $\varepsilon_f/|\mathbf{p}_f|$. This prefactor was omitted in the previous studies due to a mistake in the derivation. Because of this, all numerical results for the cross sections in Refs. [3, 4] should be multiplied by $\varepsilon_f/|\mathbf{p}_f|$. The numerical value of this prefactor is different for different initial electron energies as well as different nuclear charges. In the particular case of uranium and the incoming electron energy $T_i = 1300$ keV, the additional prefactor amounts to ≈ 1.4 .

The evaluation of the matrix elements of the operator $I(\omega)$ in Eq. (4) has been discussed in detail in Refs. [3, 4], so it need not be repeated here.

B. Effects of atomic target

In Sec. II A we studied the NCDR process in the rest frame of the nucleus, assuming that the incoming electron is free and has a definite energy and asymptotic momentum. We now consider a more realistic scenario, in which the initial-state electron is bound in a light atomic target. In the laboratory frame, the atomic target is at rest, whereas the bare nucleus (projectile) is moving with the reduced velocity $\beta = v/c$ and the Lorentz factor $\gamma = (1 - \beta^2)^{-1/2}$ along the z axis.

We shall assume that the projectile velocity β is much larger than the typical value of $|\mathbf{q}|/m$, \mathbf{q} being the momentum of a target electron with respect to the target nucleus. Under this assumption, the so-called impulse approximation [15] is valid,

which describes the atomic target as a collection of independent free electrons with a momentum distribution determined by the bound electron orbitals in the target.

From now on, we shall distinguish between the laboratory frame (unprimed variables) and the projectile frame, i.e., the nucleus rest frame (primed variables).

Within the impulse approximation, the double differential cross section of the NCDR process with capture from the atomic state $|i\rangle \equiv |njl m\rangle$ can be written as [see Ref. [2], Eq. (3.4)] as

$$\frac{d^2\sigma'}{d\Omega'_f d\varepsilon'_f} = \frac{1}{2j+1} \sum_m \int d\mathbf{q} |\psi_{njlm}(\mathbf{q})|^2 \frac{d\sigma(p'_i)}{d\Omega'_f} \times \delta(\varepsilon'_f + \varepsilon'_a + \varepsilon'_b - \varepsilon'_i), \quad (8)$$

where $\psi_{njlm}(\mathbf{q})$ is the momentum representation of the target electron wave function (in laboratory frame) and $d\sigma(p'_i)/d\Omega'_f$ is the single differential NCDR cross section as given by Eq. (4). The δ -function expresses the energy conservation in the projectile frame between the initial-state electron energy ε'_i and the emitted positron energy ε'_f .

In the laboratory frame, the initial-state electron has the energy $\varepsilon_i \equiv m - E_{i0}(i)$ and momentum \mathbf{q} . In the projectile system, the energy of the electron is $\varepsilon'_i = \gamma\varepsilon_i - \gamma v q_z$, where q_z is the projection of \mathbf{q} on the direction of the projectile propagation. We can thus rewrite the δ function in Eq. (8) as

$$\delta(\varepsilon'_f + \varepsilon'_a + \varepsilon'_b - \varepsilon'_i) = \delta(\varepsilon'_f - \varepsilon'_{f,0} + \gamma E_{i0}(i) + \gamma v q_z), \quad (9)$$

where $\varepsilon'_{f,0} = \gamma m c^2 - \varepsilon'_a - \varepsilon'_b$. Integration over q_z in Eq. (8) can be performed with help of the δ function. The result is

$$\frac{d^2\sigma'}{d\Omega'_f d\varepsilon'_f} = \frac{1}{2j+1} \sum_m \frac{1}{\gamma v} \int d^2\mathbf{q}_\perp |\psi_{njlm}(\mathbf{q})|^2 \frac{d\sigma(p'_i)}{d\Omega'_f}, \quad (10)$$

where the integration is performed over the transverse momentum \mathbf{q}_\perp , whereas the value of the longitudinal momentum is fixed by $q_z = [\varepsilon'_{f,0} - \varepsilon'_f - \gamma E_{i0}(i)]/\gamma v$.

Taking into account that the momentum distribution of the target electrons is peaked around $\mathbf{q} \approx 0$ and that the cross section only weakly depends on the direction of \mathbf{q} , we can move the cross section outside the integral,

$$\frac{d^2\sigma'}{d\Omega'_f d\varepsilon'_f} = \frac{1}{\gamma v} \frac{d\sigma(p'_i)}{d\Omega'_f} \mathcal{L}_{njl}(q_z), \quad (11)$$

where

$$\mathcal{L}_{njl}(q_z) = \frac{1}{2j+1} \sum_m \int d^2\mathbf{q}_\perp |\psi_{njlm}(\mathbf{q})|^2 \quad (12)$$

is the Compton profile of the target electron state $|njl\rangle$. We now take into account that $d^2\mathbf{q}_\perp = q_\perp dq_\perp d\varphi = q dq d\varphi$, where $q = |\mathbf{q}| = \sqrt{q_z^2 + \mathbf{q}_\perp^2}$. The integration over the polar angle in Eq. (12) is performed by using the identity

$$\frac{1}{2j+1} \sum_m |\psi_{njlm}(\mathbf{q})|^2 = \frac{1}{4\pi} [g_{njl}^2(q) + f_{njl}^2(q)], \quad (13)$$

where $g_{njl}(q)$ and $f_{njl}(q)$ are the upper and the lower radial wave-function components in the momentum representation. In the result, we have the Compton profile of the electron state $|njl\rangle$

$$\mathcal{L}_{njl}(q_z) = \frac{1}{2} \int_{q_z}^{\infty} q dq [g_{njl}^2(q) + f_{njl}^2(q)], \quad (14)$$

which is normalized as

$$2 \int_0^{\infty} dq_z \mathcal{L}_{njl}(q_z) = 1. \quad (15)$$

Finally, since we are interested in the cross section of the NCDR process, independent of the atomic shell from which the electron is captured, we need to sum up over all occupied atomic shells of the target,

$$\frac{d^2\sigma'}{d\Omega'_f d\varepsilon'_f} = \frac{1}{\gamma v} \sum_a g_a \frac{d\sigma(p'_i)}{d\Omega'_f} \mathcal{L}_a(q_z), \quad (16)$$

where g_a is the occupation number of the shell a .

C. Transformation to the laboratory frame

So far, we considered the NCDR cross section in the projectile frame. In order to provide results that can be interpreted in an experiment, we need to transform our formulas to the laboratory frame. The well-known Lorentz transformation rules from the projectile frame (primed variables) to the laboratory frame (unprimed variables) are

$$p_f \sin \theta_f = p'_f \sin \theta'_f, \quad (17)$$

$$p_f \cos \theta_f = \gamma(p'_f \cos \theta'_f + \beta \varepsilon'_f/c), \quad (18)$$

$$\varepsilon_f = \gamma(\varepsilon'_f + v p'_f \cos \theta'_f), \quad (19)$$

where θ_f is the polar angle with respect to the direction of movement of the projectile frame.

The transformation of the double-differential cross section (16) to the laboratory frame is given by (see Eq. (2.49) of Ref. [1]),

$$\frac{d^2\sigma}{d\Omega_f d\varepsilon_f} = \frac{p_f}{p'_f} \left(\frac{d^2\sigma'}{d\Omega'_f d\varepsilon'_f} \Big|_{\theta'_f \rightarrow \pi - \theta'_f} \right), \quad (20)$$

where $\theta'_f \rightarrow \pi - \theta'_f$ refers to the additional mirror reflection of the angle in the projectile frame. This reflection is needed since the propagation direction of the projectile in the laboratory system is opposite to the propagation direction of the incoming electron in the projectile system.

From Eqs. (17) and (18) we obtain

$$\frac{p_f}{p'_f} = \frac{\sin \theta'_f}{\sin \theta_f} = [\gamma^2 (g + \cos \theta'_f)^2 + \sin^2 \theta'_f]^{1/2}, \quad (21)$$

where $g = \beta/\beta'_f \equiv \beta \varepsilon'_f/(p'_f c)$.

An interesting feature of the NCDR process is the absence of the one-to-one correspondence between the angles in the

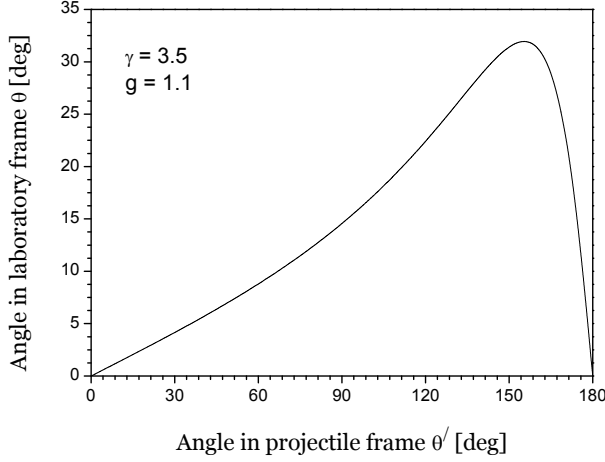


FIG. 2: Transformation of angles between the projectile frame and the laboratory frame, for collision $U^{92+} + \text{Ar}$ at 2.37 GeV/u, at the maximum of the positron-energy spectrum.

projectile and in the laboratory frame. The reason is that for NCDR the reduced velocity of the projectile system β is larger than the reduced velocity of the emitted positron in the projectile frame β'_f , i.e., $g > 1$. The typical angle transformation plot in this case is shown in Fig. 2. From this figure we observe, first, that the positron emission angle in the laboratory systems cannot exceed some maximal value θ_{\max} with $\tan \theta_{\max} = 1/(\gamma\sqrt{g^2 - 1})$ and, second, that any angle $\theta_f \neq \theta_{\max}$ in the laboratory frame corresponds to *two* angles in the projectile frame, $\theta'_{f,1}$ and $\theta'_{f,2}$ [16]. Moreover, from Eq. (19) we deduce that the positron energy in the laboratory frame ε_f depends on the emission angle in the projectile system θ'_f . Therefore, every peak of the positron energy spectrum in the projectile system is transformed into *two* peaks in the laboratory frame.

For completeness, we also present the Lorentz transformation of the angle-differential NCDR cross section (4) from the projectile frame into the laboratory frame,

$$\frac{d\sigma}{d\Omega_f} = \left| \frac{d \cos \theta'_f}{d \cos \theta_f} \right| \left(\frac{d\sigma'}{d\Omega'_f} \Big|_{\theta'_f \rightarrow \pi - \theta'_f} \right), \quad (22)$$

where the Jacobian of angle transformation is given by

$$\left| \frac{d \cos \theta'_f}{d \cos \theta_f} \right| = \frac{[\gamma^2(g + \cos \theta'_f)^2 + \sin^2 \theta'_f]^{3/2}}{\gamma|1 + g \cos \theta'_f|}. \quad (23)$$

The transformation (22) is encountered if we assume (as in Refs. [3, 4]) the asymptotic momentum of the incoming electron to be fixed, i.e., if we neglect the momentum distribution of the electrons in the target.

It is remarkable that the angle transformation (23) is singular for $g \geq 1$, as the denominator vanishes at the critical angle $\cos \theta'_{\max} = -1/g$. In contrast to that, the angle transformation for the double differential cross section (21) does not contain any singularities. (The singularity may be recovered if

we assume a δ -function energy distribution of target electrons and integrate over the electron energy.) In the present work we will demonstrate that the singularity of the cross section in the laboratory frame disappears if we assume any reasonable momentum distribution of target electrons.

III. NUMERICAL DETAILS

The evaluation of the angle-differential NCDR cross section $d\sigma/d\Omega_f$ defined by Eq. (4) was discussed in detail in Refs. [3, 4] and thus will not be repeated here. In the present work we need to convolute the the angle-differential cross section with the Compton profile of the target atomic orbitals \mathcal{L}_a , given by Eq. (14). We compute the Compton profile \mathcal{L}_a by first solving the Dirac-Fock equation for the neutral atomic target and then performing a numerical Fourier transform of these Dirac-Fock orbitals. The numerical Fourier transform was computed by using the routines for the sine and cosine transforms from NAG library. Finally, the momentum integration in Eq. (14) was evaluated by using the Gauss-Legendre quadratures. The obtained Compton profile $\mathcal{L}_a(q_z)$ was stored on a q_z grid and then interpolated to allow a smooth convolution.

IV. RESULTS AND DISCUSSION

We start with examining the angle-differential cross section, which is obtained in the laboratory frame by integrating the double-differential cross section (20) over all energetically possible positron energies,

$$\frac{d\sigma}{d\Omega_f} = \int d\varepsilon_f \frac{d^2\sigma}{d\Omega_f d\varepsilon_f}. \quad (24)$$

Let us first consider the dominant NCDR channel, with capture into the ground $(1s)^2$ state of the final ion. In Fig. 3 we present a plot of the angle-differential NCDR cross section as defined by Eq. (24) in the laboratory frame for the collision of bare uranium U^{92+} at 2.37 GeV/u with two neutral targets, Ar (left graph) and He (right graph) and for the capture into the $(1s)^2$ final state of U^{90+} . As the cross sections for different targets are roughly proportional to the number of target electrons, both graphs looks quite similar, apart from the scaling factor of $18/2 = 9$.

In Fig. 3, we compare the results that include the momentum distribution of the electrons in the target (solid line) with the results obtained under the assumption that the initial electron is free and has a fixed asymptotic momentum and energy $\varepsilon_i = \gamma mc^2$ (dashed line). We note that in the latter case the cross section needs to be multiplied by the number of electrons in the target, to be directly comparable to the results of the full calculation. As seen from the figure, the agreement between the two approaches is very good except in the region close to the critical angle θ_{\max} . If the initial electron has fixed energy and momentum, the laboratory angle cannot exceed θ_{\max} and the differential cross section is divergent at this

point. If we take into account the momentum distribution of the target electrons, however, the singularity of the cross section is replaced by a distorted bell-shape of the Compton profile. In addition, emission to the region of $\theta_f > \theta_{\max}$ becomes possible, although the cross section is small in this region and decreases fast as the angle is increased. As expected, we find a close relation between the width of the Compton profile of the target and the relative value of the maximum of the peak at $\theta_f = \theta_{\max}$: the sharper the profile, the higher the peak in the differential cross section.

We observe that the enhancement of the cross section in the angular region around $\theta_f = \theta_{\max}$ is not very pronounced and that the maximum of the cross section is reached at the forward angle $\theta_f = 0^\circ$ of the laboratory frame. This makes the forward emission to be most suitable for determining the NCDR process experimentally. Moreover, the forward angle seems to be most convenient from the experimental point of view, since the planned setup of the HESR facility involves a high-resolution forward-emission spectrometer [10].

In Fig. 4 we plot the angle-differential cross section of the NCDR process for the forward positron emission angle $\theta_f = 0^\circ$ as function of the projectile energy, for capture into different states of the final ion. In the present work, we performed numerical calculations of the NCDR cross sections with capture into all singly excited states of the form $(1snl_j)_J$ with $n \leq 4$ and double excited states $(2s2l_j)_J$, altogether 36 different NCDR channels. Following to Ref. [4], we observe that the dominant contribution comes from the capture into the ground $(1s)^2$ state. The second and third largest contributions come from the capture into the $(1s2s)_0$ and $(1s3s)_0$ states; all other channels give rise to much smaller contributions.

The energy dependence of the forward-emission NCDR cross section is qualitatively the same as for the total NCDR cross section. It rapidly increases above the threshold energy, has the flat maximum at about 2.25 GeV/u and later falls off slowly if the projectile energy is further enlarged. From this we conclude that the region of projectile energies 2-2.5 GeV/u is the most suitable for experimental determination of the NCDR process.

We now turn to examining the NCDR spectrum of the double differential cross section (20) as function of the positron energy. From the discussion above, we may anticipate that, for a given positron emission angle, the positron-energy NCDR spectrum has peaks, whose centroid energies are determined by the binding energy of the final ion state and whose widths are shaped by the Compton profile of the target atom. In addition, we may expect that in the laboratory frame, capture into each final state is represented by *two* peaks of the positron-energy spectrum.

Fig. 5 shows the positron-energy spectrum of the NCDR cross section in the laboratory frame for the forward positron emission angle $\theta_f = 0^\circ$, for scattering of U^{92+} at 2.37 GeV/u on two atomic targets, Ar and He. The dominant NCDR chan-

nel of capture into the ground $(1s)^2$ shell is labelled as “KK”. As expected, we find two “KK” peaks in the spectrum. The most prominent peak at about 6.4 MeV corresponds to the forward positron emission in the projectile frame. The second “KK” peak corresponding to the positron backward emission in the projectile frame is much weaker and is suppressed by more than an order of magnitude. The individual $(1s2l_j)_J$ peaks in the positron-energy NCDR spectrum cannot be resolved even in the case of the helium target; the corresponding total peak is labelled as “KL”. The contributions of higher excited final states to the positron-energy spectrum are even smaller and are almost indiscernible on the graphs.

The shape of the positron-energy NCDR spectrum changes if the observation angle in the laboratory frame is increased. Fig. 6 shows the positron-energy NCDR spectrum for the positron emission angle $\theta_f = 20^\circ$. We observe that the forward- and backward-scattering peaks are now much closer to each other and that the ratio of intensities of these peaks is now much (by about 5 times) smaller.

The change of the shape of the spectrum becomes even more pronounced if we increase the observation angle further. Fig. 7 shows the positron-energy NCDR spectrum for the positron emission angle $\theta_f = 27^\circ$. We see that the two “KL” peaks merge into one double-humped peak and that the two “KK” peaks move very close to each other and to the “KL” double-peak. For such a large angle, the intensities of the forward- and backward-scattering peaks become almost equal.

V. SUMMARY

In summary, we have studied the process of the negative-continuum assisted dielectronic recombination (NCDR) that occurs in collision of a heavy bare nucleus with light target atoms. The single and double-differential cross sections of the positron production in the NCDR process have been calculated within the relativistic framework based on QED theory. Different channels of the NCDR process have been considered explicitly, including the capture into 36 low-lying states of the final ion. Special attention has been paid to the effects of the atomic targets upon the spectra of the emitted positrons. It has been demonstrated, in particular, that the target effects remove the non-physical singularity of the differential cross section, which occurs for the initially monochromatic electrons.

Acknowledgements

This work is supported by BMBF project 05P15SJFAA. V.A.Y. acknowledges support by the Russian Federation program for organizing and carrying out scientific investigations.

[1] J. Eichler and W. Meyerhof, *Relativistic Atomic Collisions*, Academic Press, San Diego, 1995.

[2] J. Eichler and T. Stöhlker, Phys. Rep. **439**, 1 (2007).

[3] A. N. Artemyev, T. Beier, J. Eichler, A. E. Klasnikov,

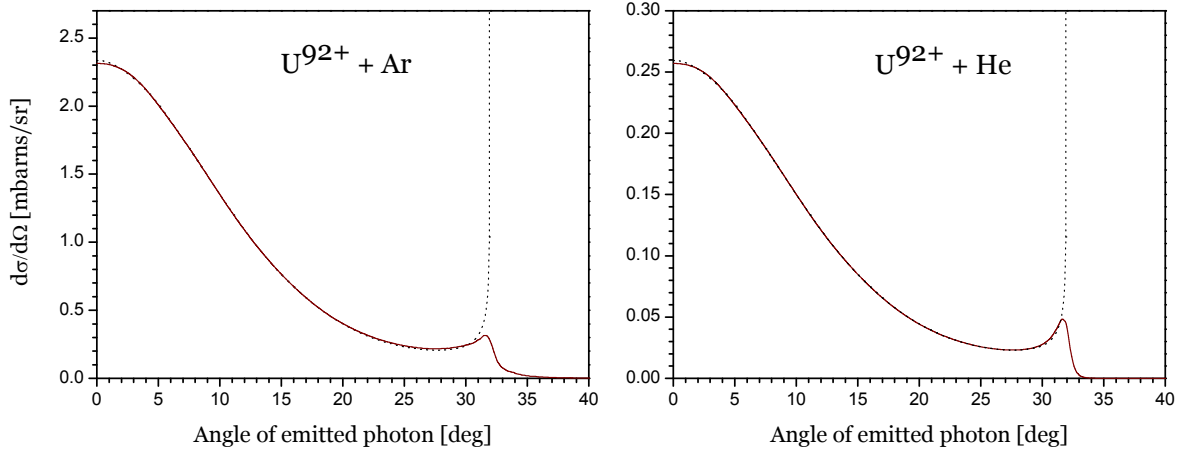


FIG. 3: (Color online) Angle-differential cross section of the NCDR process as a function of the emission angle of the outgoing positrons in the laboratory frame. Results are shown for the scattering of U^{92+} on Ar (left graph) and He (right graph) with capture into the $(1s)^2$ final state of U^{90+} , for the projectile energy of 2.37 GeV/u. The solid line denotes the results of the full calculation including the Compton profile [Eq. (24)], whereas the dotted line displays data as obtained for the initially monochromatic incoming electrons.

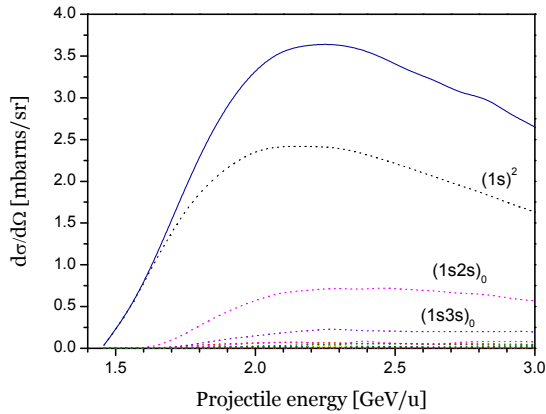


FIG. 4: (Color online) Angle-differential cross section of the NCDR process at fixed emission angle $\theta_f = 0^\circ$ of the positrons in the laboratory frame. Theoretical results are shown as function of the projectile energy, for the collision of U^{92+} on Ar. The dashed lines denote contributions of capture into different individual final states of U^{90+} , whereas the solid line refers to the sum of all individual contributions.

C. Kozhuharov, V. M. Shabaev, T. Stöhlker, and V. A. Yerokhin, Phys. Rev. A **67**, 052711 (2003).

- [4] A. N. Artemyev, V. M. Shabaev, T. Stöhlker, and A. S. Surzhykov, Phys. Rev. A **79**, 032713 (2009).
- [5] R. H. Bell and M. J. Seaton, J. Phys. B **18**, 1589 (1985).
- [6] Y. Hahn and K. Lagattuta, Physics Reports **166**, 195 (1988).

- [7] W. Spies, A. Müller, J. Linkemann, A. Frank, M. Wagner, C. Kozhuharov, B. Franzke, K. Beckert, F. Bosch, H. Eickhoff, M. Jung, O. Klepper, W. König, P. H. Mokler, R. Moshhammer, F. Nolden, U. Schaaf, P. Spädtke, M. Steck, P. Zimmerer, N. Grün, W. Scheid, M. S. Pindzola, and N. R. Badnell, Phys. Rev. Lett. **69**, 2768 (1992).

- [8] C. Brandau, C. Kozhuharov, A. Müller, W. Shi, S. Schippers, T. Bartsch, S. Böhm, C. Böhme, A. Hoffknecht, H. Knopp, N. Grün, W. Scheid, T. Steih, F. Bosch, B. Franzke, P. H. Mokler, F. Nolden, M. Steck, T. Stöhlker, and Z. Stachura, Phys. Rev. Lett. **91**, 073202 (2003).

- [9] C. Brandau, C. Kozhuharov, Z. Harman, A. Müller, S. Schippers, Y. S. Kozhedub, D. Bernhardt, S. Böhm, J. Jacobi, E. W. Schmidt, P. H. Mokler, F. Bosch, H.-J. Kluge, T. Stöhlker, K. Beckert, P. Beller, F. Nolden, M. Steck, A. Gumberidze, R. Reuschl, U. Spillmann, F. J. Currell, I. I. Tupitsyn, V. M. Shabaev, U. D. Jentschura, C. H. Keitel, A. Wolf, and Z. Stachura, Phys. Rev. Lett. **100**, 073201 (2008).

- [10] P.-M. Hillenbrand, S. Hagmann, K. E. Stiebing, S. Schippers, Y. A. Litvinov, and T. Stöhlker, Phys. Scr. (2015), to be published.

- [11] B. Najjari, A. B. Voitkov, A. Artemyev, and A. Surzhykov, Phys. Rev. A **80**, 012701 (2009).

- [12] C. Itzykson and J. Bernard Zuber, *Quantum Field Theory*, McGraw-Hill, NY, 1980.

- [13] J. D. Bjorken and S. D. Drell, *Relativistic Quantum Mechanics*, McGraw-Hill, NY, 1964.

- [14] V. M. Shabaev, Phys. Rep. **356**, 119 (2002).

- [15] M. Kleber and D. H. Jakubassa, Nucl. Phys. **252**, 152 (1975).

- [16] K. G. Dedrick, Rev. Mod. Phys. **34**, 429 (1962).

- [17] Conceptual Design Report, <http://www-alt.gsi.de/documents/FOLDER-1080>

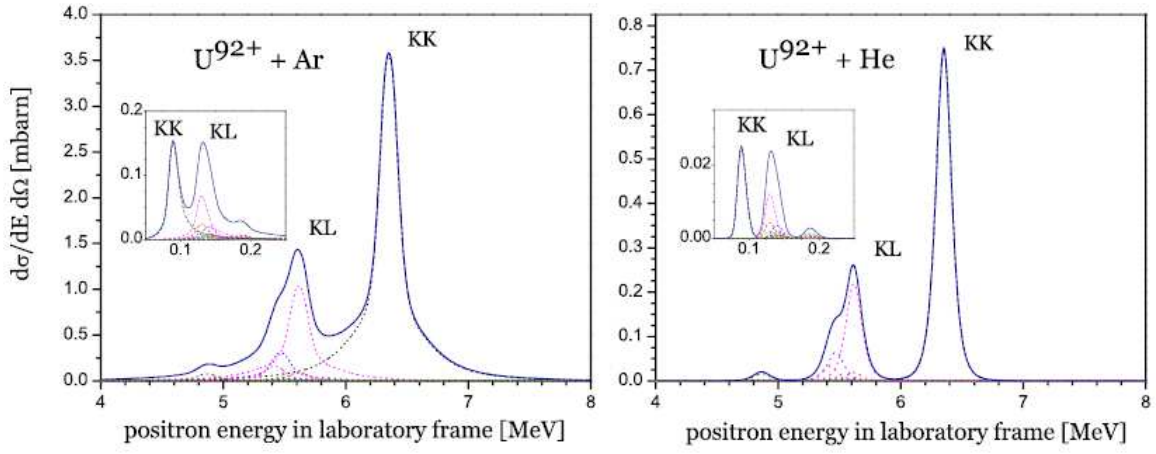


FIG. 5: (Color online) Double-differential cross section of the NCDR process as function of the positron energy in the laboratory system, for the positron emission angle fixed of $\theta_f = 0^\circ$. Results are shown for the scattering of U^{92+} at 2.37 GeV/u on Ar (left graph) and He (right graph). The solid line denotes the total cross section, whereas the dotted lines denote individual contributions of capture into different final states of U^{90+} .

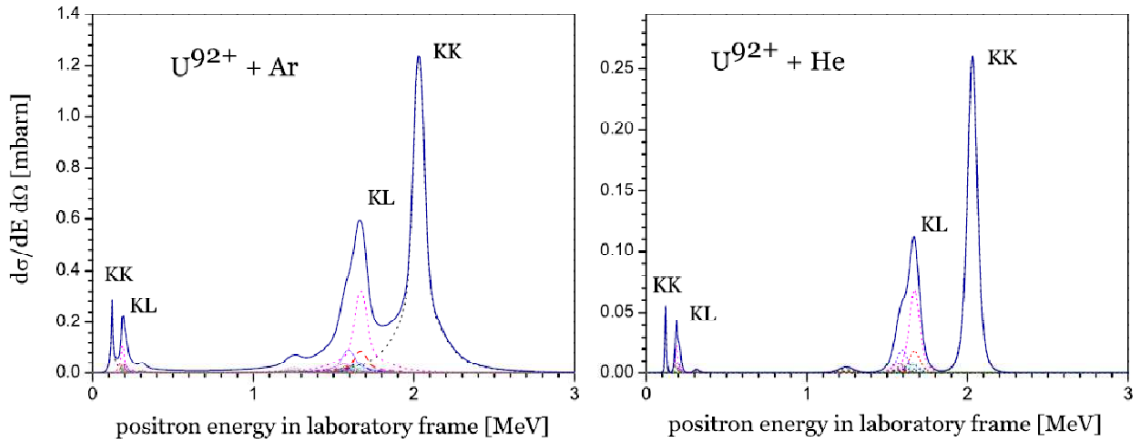


FIG. 6: (Color online) The same as Fig. 5 but for $\theta_f = 20^\circ$.

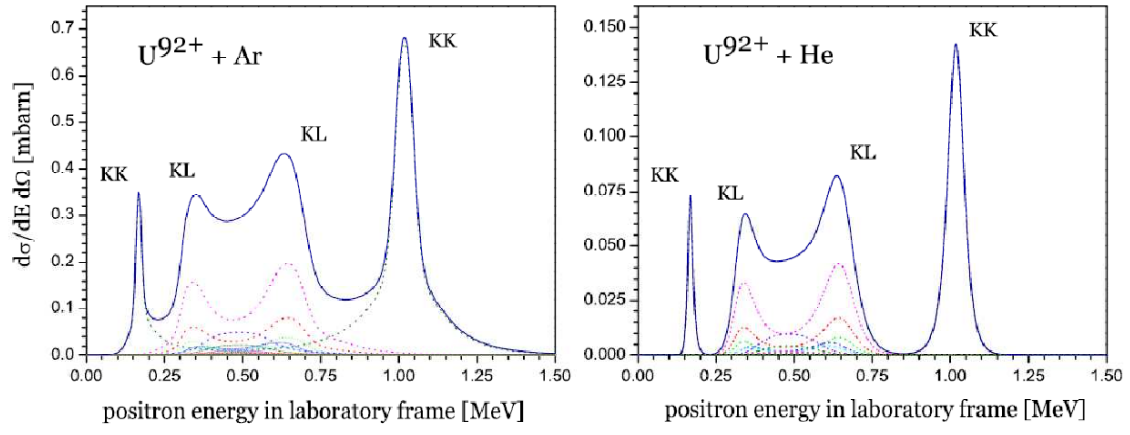


FIG. 7: (Color online) The same as Fig. 5 but for $\theta_f = 27^\circ$.